frontiers | Frontiers in Earth Science

TYPE Original Research
PUBLISHED 31 May 2023
DOI 10.3389/feart.2023.1137416

OPEN ACCESS

EDITED BY
Kristen Fauria,
Vanderbilt University, United States

REVIEWED BY
Calvin F. Miller,
Vanderbilt University, United States
Sean O'Donnell,
The University of Texas at Austin, United States
Takeshi Kuritani,
Hokkaido University, Japan

*CORRESPONDENCE
Yoshihiko Tamura,
tamuray@jamstec.go.jp

RECEIVED 04 January 2023
ACCEPTED 09 May 2023
PUBLISHED 31 May 2023

CITATION
Tamura Y, Sato T, Ishizuka O, McIntosh IM, Yoshida K, Maeno F and Chang Q (2023), Genesis and interaction of magmas at Nishinoshima volcano in the Ogasawara arc, western Pacific: new insights from submarine deposits of the 2020 explosive eruptions.
Front. Earth Sci. 11:1137416.
doi: 10.3389/feart.2023.1137416

Genesis and interaction of magmas at Nishinoshima volcano in the Ogasawara arc, western Pacific: new insights from submarine deposits of the 2020 explosive eruptions

Yoshihiko Tamura[1]*, Tomoki Sato[1], Osamu Ishizuka[2], Iona M. McIntosh[1], Kenta Yoshida[1], Fukashi Maeno[3] and Qing Chang[1]

[1]Research Institute for Marine Geodynamics (IMG), Japan Agency for Marine-Earth Science and Technology (JAMSTEC), Yokosuka, Japan, [2]Geological Survey of Japan, National Institute of Advanced Industrial Science and Technology (AIST), Tsukuba, Japan, [3]Earthquake Research Institute, The University of Tokyo, Tokyo, Japan

Sudden changes of eruption styles and magma compositions at arc volcanoes are enigmatic processes. Nishinoshima volcano, western Pacific, has had historical eruptions in 1973–1974 and from 2013 on and off to the present day. These eruptions were characterized by effusive Strombolian eruptions of andesite magmas until mid-June 2020, when they suddenly transitioned to violent explosive Strombolian eruptions that produced tephra fallout over a wide area. To understand this transition, we conducted marine surveys and sampling of the extensive submarine deposits of the tephra fallout. Our new data demonstrate that the full compositional range of the 2020 eruptions spans from basalt to dacite. We present evidence for magma mixing of newly injected basalt with andesite magmas. Nishinoshima consists of an andesitic main edifice surrounded by basaltic knolls: previous studies have shown that Nishinoshima andesite compositions can be generated by olivine fractionation of primary andesitic magmas that result from partial melting of hydrous mantle at relatively low pressures under the thin crust of the Ogasawara arc; knoll basalt compositions can be generated by partial melting of mantle at greater depths and were interpreted as older events of the volcano. We show that basalt magmas could have been generated throughout the entire history of Nishinoshima. In addition, we show that andesites from Nishinoshima and nearby Nishinoshima-Minami Knoll, which are only ~8 km apart, have distinct subduction components. Together, these data improve our understanding of the diverse primary magmas responsible for the construction and continuing eruptive activity of an active island arc volcano.

KEYWORDS

basalt, andesite, mission immiscible, magma mixing, violent eruption, new continent

1 Introduction

Sudden changes of eruption styles and magma compositions at arc volcanoes are enigmatic processes that must be better understood in order to prepare for volcanic disasters. Recent eruptions of Nishinoshima volcano, a highly active island arc volcano in the Izu-Ogasawara arc in the western Pacific, have exhibited such a change in eruption style and magma composition. These recent eruption deposits therefore provide important geochemical data for investigating this phenomenon.

The Izu-Ogasawara arc extends for 1,330 km between the island of Honshu, Japan, and the northern part of the Mariana arc. It consists of 21 active island volcanoes and submarine volcanoes, from Izu-Oshima Island in the north to Nikko Seamount in the south (https://www.data.jma.go.jp/vois/data/tokyo/STOCK/souran_eng/menu.htm) (Figure 1). The arc results from the subduction of old ocean floor (135–180 Ma) of the western Pacific Plate beneath the Philippine Sea Plate along the Izu-Ogasawara Trench. In the Ogasawara segment of the arc (south of ~30°N), the crust is divided by the Ogasawara Trough into the Eocene–Oligocene Ogasawara Ridge, including Chichijima island, and the present active Ogasawara arc, which has thin underlying crust (16–21 km, Kodaira et al., 2007) and consists mostly of submarine volcanoes.

Nishinoshima, a small island located ~1,000 km south of Tokyo in this active Ogasawara arc, is the subaerial summit of a much larger submarine volcano. The existence of this island has been known since 1702 (Aoki and Ossaka, 1974), but its first recorded eruption was in 1973. Following a lull of four decades, it suddenly began erupting again in November 2013 and activity has continued on and off until the present day.

A previous study (Tamura et al., 2019) reported whole rock geochemistry of lavas and scoria dredged from the main submarine volcanic edifice in 2015 (eruption age unknown) and subaerial lava blocks from the 2015 eruption sampled by unmanned helicopter. Both the submarine and subaerial samples are andesitic in composition (58–62 wt% SiO_2), and similar to the andesitic composition of the 1973 eruption products and pre-1973 edifice (Osaka, 1973; Osaka, 1974; Osaka, 1975; Osaka et al., 1974; Aoki et al., 1983; Ishizuka et al., 2007; Umino and Nakano, 2007). The crust underlying Nishinoshima volcano is 21 km thick, without any thinning due to rifting, and thus Nishinoshima is one of the closest arc volcanoes to the mantle on the Earth (Kodaira et al., 2007). Tamura et al. (2016) showed a relationship between crustal thickness and magma type in the Izu-Ogasawara and Aleutian oceanic arcs, where volcanoes on thin crust erupt predominantly andesitic magmas whereas volcanoes on thick crust erupt predominantly basaltic magmas. To explain this relationship Tamura et al. (2016) reviewed geochemical and petrological data and hypothesized that where the crust is thin, partial melting of hydrous mantle occurs at low pressure below the thin crust, producing andesitic primary magmas. Where the crust is thick, melting pressures are higher and only basaltic magmas tend to be produced. Although this may seem counter-intuitive, the implications of this hypothesis are: 1) the rate of continental crust accumulation, which is andesitic in composition, would have been greatest soon after subduction initiated on Earth, when most crust was thin; and 2) most andesite magmas erupted on continental crust could be recycled from "primary" andesite originally produced in oceanic arcs (Tamura et al., 2016). The geochemical data from the Nishinoshima andesites collected in and prior to 2015 have been interpreted as evidence for this process occurring at Nishinoshima volcano, i.e., the andesite magmas derive from a shallow mantle source (Tamura et al., 2019).

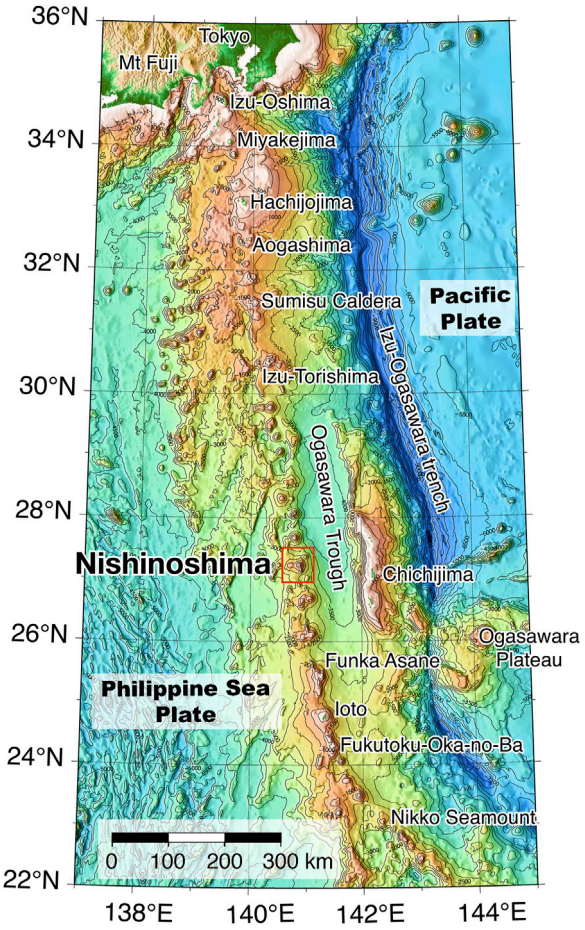

FIGURE 1
Bathymetric features of the Izu-Ogasawara arc system. Old ocean floor (135–180 Ma) of the western Pacific Plate is subducting beneath the active Izu-Ogasawara arc at the Izu-Ogasawara Trench. This island arc has 21 active island and submarine volcanoes from Izu-Oshima in the north to Nikko Seamount in the south (https://www.data.jma.go.jp/vois/data/tokyo/STOCK/souran_eng/menu.htm). The Ogasawara Trough divides the Ogasawara arc crust into the Eocene–Oligocene Ogasawara Ridge, including Chichijima, and the present Ogasawara arc, which has thin underlying crust (16–21 km) and consists mostly of submarine volcanoes. The map was created by using GMT v. 5.1.1 (http://gmt.soest.hawaii.edu/). Numbers on the contour lines are in meters. Nishinoshima means Western Island in Japanese, which could be a reference to the location of the island, approximately 130 km west of Chichijima.

Since the 2015 submarine and subaerial sampling Nishinoshima has continued to erupt, including a transition to more explosive activity. Maeno et al. (2021) reported the detailed sequence of Nishinoshima's eruptive activity from 2013 to 2020, which can be divided into four episodes (Figure 2A). The duration of the eruptive episodes was initially 2 years (Episode 1), and 120 days (Episode 2), but shortened to a week by Episode 3, with decreasing

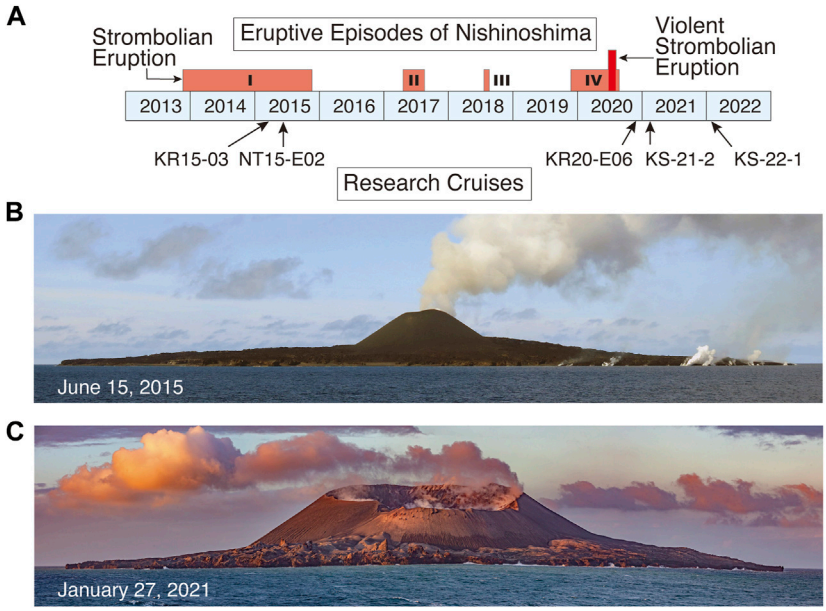

FIGURE 2
(A) Eruptive episodes of Nishinoshima and the timing of JAMSTEC research cruises. The duration of the eruptive episodes was initially 2 years (Episode 1), and 120 days (Episode 2), but shortened to a week by Episode 3, with decreasing eruptive volume with time. The Episode 4 lasted for 270 days. The eruption style changed in mid-June 2020 from mostly effusive Strombolian to violent Strombolian, after which eruption columns continuously reached a height of 2–6 km (maximum 8 km) and a large amount of tephra fall out occurred over more than several tens of kilometer from the island (Yanagisawa et al., 2020). We sampled the Nishinoshima area in February 2015, June 2015, December 2020, January 2021, and January 2022, during the JAMSTEC cruises KR15-03, NT15-E02, KR20-E06, KS-21-2, and KS-22-1, respectively. **(B)** Nishinoshima seen from the west on 15 June 2015, during NT15E-02. The height of the central cone is ~150 m. **(C)** Nishinoshima seen from the south on 27 January 2021, during KS-21-2. The height of the central cone is ~250 m (photographed by Chong Chen).

eruptive volume with time. Something, however, changed from 2019 to 2020 during Episode 4, which lasted for 270 days. The average effusion rates for the 2013–2015 eruption (Episode 1) and the 2017 eruption (Episode 2) were estimated to be 2.0×10^5 m^3/day and 1.5×10^5 m^3/day, respectively (Maeno et al., 2016; Maeno et al., 2021; Kaneko et al., 2019). The activity that began in December 2019 (Episode 4) however was intense, with a maximum magma discharge rate of 2.6×10^6 m^3/day (Maeno et al., 2021; Kaneko et al., 2022). Moreover, in June 2020 the eruption style switched from mostly effusive Strombolian to violent Strombolian, during which time eruption columns continuously reached a height of 2–6 km (maximum 8 km) and a large amount of tephra fall out occurred extending several tens of kilometers from the island (Yanagisawa et al., 2020). Long-term geochemical monitoring of 2013–2020 subaerial eruption products showed that this transition in eruption style was associated with a change from the initial andesite magma with ~60 wt% SiO_2 to a more mafic basaltic andesite magma with ~55 wt% SiO_2 in Episode 4 (Maeno et al., 2021). After Episode 4, small eruptions were observed by a weather satellite in October 2022 and by an aircraft of the Japan Coast Guard in January 2023.

Following the Episode 4 transition in eruption style and magma composition we returned to the Nishinoshima area to conduct further submarine survey and sampling (JAMSTEC cruises KR20-E06 in December 2020, KS-21-2 in January 2021, and KS-22-1 in January 2022; Figure 2A). Figures 2B, C show Nishinoshima island in profile on 15 June 2015 and 27 January 2021, as seen from the ship during the previous 2015 NT15E-02 cruise (Tamura et al., 2019) and 2021 KS-21-2 cruise, respectively. There were drastic changes before and after Episode 4; the height of the central cone increased from 150 to 250 m and the crater had been enlarged from 150 to 570 m in diameter (Maeno et al., 2021). The dimensions of the island were 2.0 km from east to west and 1.8 km from north to south in May 2019. The huge volumes of lava subsequently erupted during Episode 4 increased the landmass of the island by 33 percent from 2.89 km^2 in May 2019 to ~3.9 km^2 in August 2020, according to GSI (Geospatial Information Authority of Japan) analysis of satellite images. The island now measures 2.3 km from east to west and 2.4 km from north to south.

In this study we present whole-rock geochemical data for the submarine volcanic products (plausibly from the 2019-2020 eruptions) obtained by the KR20-E06, KS-21-2 and KS-22-1 cruises. These supplement the whole-rock geochemical data of the subaerial and submarine volcanic products sampled in 2015 that have already been reported in Tamura et al. (2019). We explore the possibility that the change in erupted magma composition in 2020 from andesite to basaltic andesite reflects a change in the composition of primary magmas resulting from partial melting of the mantle, from primary andesite produced at shallow depths beneath thin crust to primary basalt produced at considerable depth. Basalt magmas have recently been shown to have triggered the 2021 explosive pumice eruption of Fukutoku-Oka-no-Ba volcano, 300 km south of Nishinoshima in the same arc (Yoshida et al., 2022), providing another example where hydrous

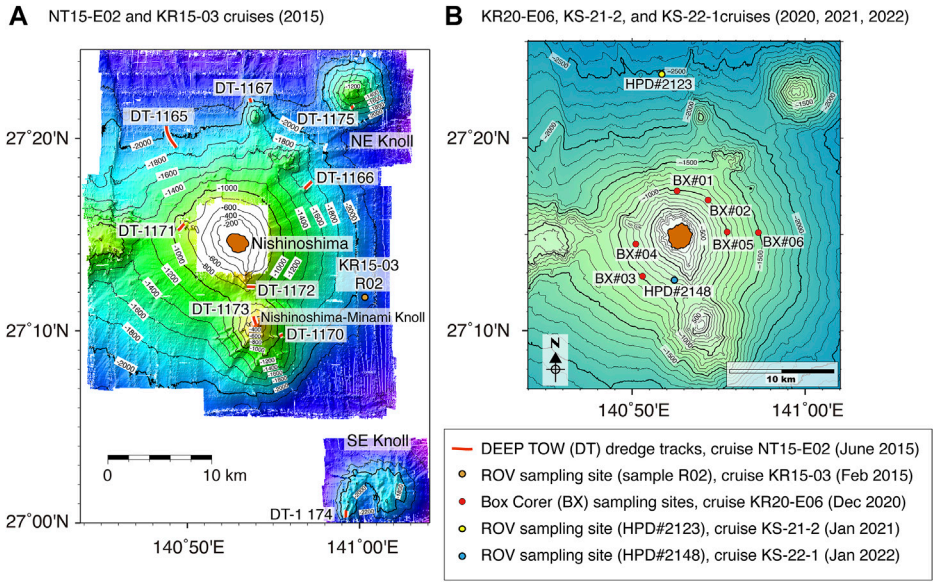

FIGURE 3
(A) The dredge tracks of the DEEP TOW system during cruise NT15-E02 in 2015. The old knolls around Nishinoshima (NE and SE Knolls) consist of basalt lavas, but the main body of the Nishinoshima volcano is andesitic in composition (Tamura et al., 2019) A loose sample collected by submersible during cruise KR15-03 in 2015 is also shown. **(B)** Red circles show sampling sites around Nishinoshima using box corer (prefix BX) during cruise KR20-E06 in 2020. Yellow circle is sampling sites ~15 km north of Nishinoshima using ROV Hyper Dolphin during cruise KS-21-2 in 2021 (denoted HPD#2123). Blue circle is sampling site ~3 km south of Nishinoshima using ROV Hyper Dolphin during cruise KS-22-1 in 2022 (denoted HPD#2148).

basaltic magmas in oceanic arcs produce explosive eruptions. In this context, our geochemical data yield new insights into the magma system of Nishinoshima volcano and the generation and interaction of magmas involved in explosive eruptions at island arc volcanoes.

2 Materials and methods

2.1 Research cruises

A brief summary of the 2015 sampling is given here; full details are given in Tamura et al. (2019). Cruise KR15-03 of R/V Kairei in February 2015 collected loose boulders ESE of Nishinoshima in water depths of 2,100 m below sea level (b.s.l.) using the remotely operated submersible KAIKO Mk-IV. Cruise NT15E-02 of R/V Natsushima in June 2015 conducted dredges using the deep ocean floor towed survey system (DEEP TOW) on the submarine flank of Nishinoshima, the summit and flank of Nishinoshima-Minami Knoll (8 km south of the island), and the steep cliffs of the adjacent NE Knoll and SE Knoll, located 18 km and 28 km from the island, respectively (Figure 3A). These dredges spanned water depths between 203 m b.s.l. and 2,060 m b.s.l. and collected lavas and scoria (Tamura et al., 2019). Finally, subaerial lava blocks from the 2015 eruption were collected using an unmanned helicopter during the cruise of the R/V Daisan Kaiyomaru in June-July 2015.

Cruise KR20-E06 of R/V Kairei in December 2020 sampled the surface sediments (very recent volcaniclastics) of the submarine flanks of Nishinoshima, from 5 to 7 km from the volcanic center and water depths between 500 m b.s.l. and 1,500 m b.s.l., using a Box Corer (Figure 3B). The Box Corer is 120 cm (width) * 130 cm (length) * 150 cm (height) and weighs 260 kg. When it reaches the seafloor, its box covers an area of 0.1 m^2 and strips the upper 10–20 cm of seafloor sediments.

Cruise KS-21-2 of R/V Shinseimaru in January 2021 sampled the surface sediments (very recent volcaniclastics) of the submarine flank of Nishinoshima at 15 km to the north of the volcanic center at a water depth of 2,500 m b.s.l. using the remotely operated submersible Hyper Dolphin (HPD#2123 in Figure 3B). The Hyper Dolphin made a video survey of the seafloor and sampled seafloor sediments using a 40 cm-long push core held by the submersible's manipulator arm.

Cruise KS-22-1 of R/V Shinseimaru in January 2022 collected additional lava fragments from the southern slope of Nishinoshima at 4 km from the volcanic center and a water depth of 790 m b.s.l. using the Hyper Dolphin manipulator arm (HPD#2148 in Figure 3B).

Samples recovered by these 2020–2022 Box Corer and Hyper Dolphin sampling surveys are deemed to be the products of the most recent Episode 4 eruptions in 2020, due to their proximity to the volcanic center and similarity to subaerial observations. The submarine outcrops observed to the north at 2,500 m b.s.l. (HPD#2123) exhibit alternate layers of white pumice and black scoria tuffs, reflecting the known bimodal nature of the Episode 4 eruptions (Figures 4A, B). Although land sampling surveys were not possible during the period of the 2020 and 2021 cruises, Maeno et al. (2021) used an aerial drone in December 2020 to show that nearly the entire lava flow field had been covered by pyroclastic deposits except for a few locations on the southwest and northwest coasts. In the north, the tephra deposit was more than 5 m thick, reflecting the northward direction of the major tephra dispersal axis

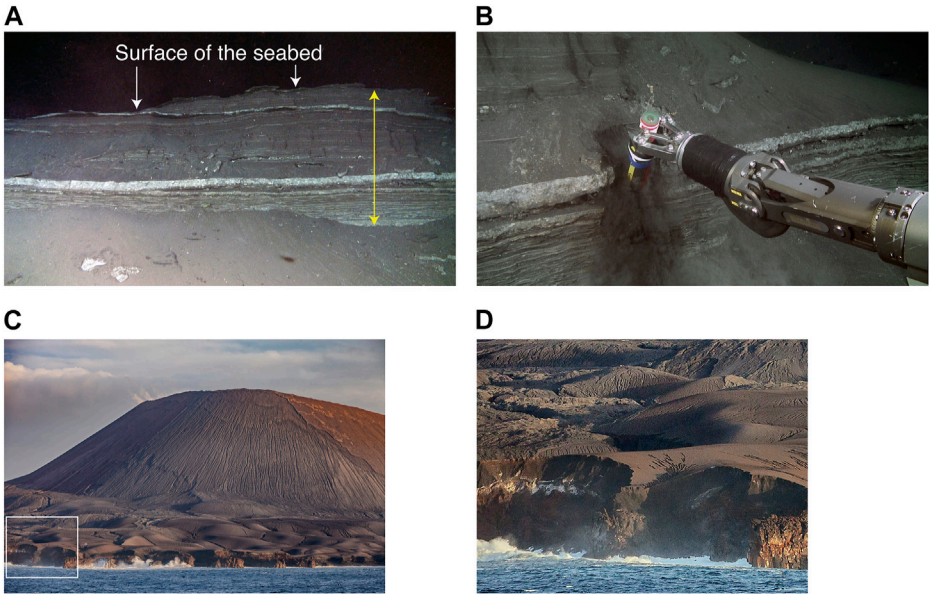

FIGURE 4
(A) Alternate layers of black and white tephra observed ~15 km north of Nishinoshima at a depth of 2,473 m b.s.l. (27°23.2934′N and 140°51.6102′E) during HPD#2123 dive of ROV Hyper-Dolphin on 23 January 2021. The yellow double-ended arrow shows a length of ~1 m. **(B)** Pushing a plastic cylinder (push-core) to sample the outcrop using Hyper-Dolphin. The layers are, however, soft, unconsolidated, and fragile and are difficult to keep in the original shape of the sediment. **(C)** Nishinoshima seen from the northwest on 27 January 2020, by Chong Chen. The white rectangle in the lower left of the photo is enlarged in **(D)**. The central cone is ~250 m in height. **(D)** An enlarged part of the previous photo, which shows the coast of Nishinoshima eroded by sea, consisting of lava flows and overlying tephra layers. Alternate bands of white and black color exist between the thick black ash layers and underlying lava flows: these tephra layers may correlate with the submarine layers 15 km away from the island shown in **(A)**.

during the explosive phase (Maeno et al., 2021). Figure 4C shows Nishinoshima taken from the northwest on 27 January 2020. The central cone is ~250 m in height. The white rectangle in the lower left of the photo is enlarged in Figure 4D. This part of the sea cliff of Nishinoshima has been eroded by the sea and consists of lava flows and overlying tephra layers. Alternate bands of white and black color exist between the overlying thick black ash layers and the underlying lava flows: we suggest these distinctive tephra layers correlate with the HPD#2123 submarine layers 15 km further to the north that are shown in Figures 4A, B.

Figures 5A, B show seafloor sediments (the uppermost tephra) from the December 2020 Box Corer samples BX#01 and BX#02, respectively, whose locations are shown in Figure 3B. Here the seafloor was mostly covered by black tephra (scoria), but some light-colored material (pumice) was observed along with the scoria. Figures 5C, D show pumice from BX#01 and scoria from BX#06, respectively. Figures 5E, F show pumice and scoria recovered from the white and black layers, respectively, sampled in January 2021 during dive HPD#2123 and seen in Figure 4B. Figures 5G, H show a sample collected in January 2022 during dive HPD#2148, and an Si X-ray map of a thin section of this sample is shown in Figure 5I.

2.2 Analytical methods

Samples with "R" in the sample number except for BX03-R05 were pulverized using a polycarbonate tube and alumina rod. Other samples were pulverized in an agate mortar. Major elements were determined on fused glass discs by XRF (ZSX Primus II, Rigaku) at Japan Agency for Marine-Earth Science and Technology (JAMSTEC) following the method of Tani et al. (2005). A mixture of ~0.4 g powdered sample and 4 g of anhydrous lithium tetraborate ($Li_2B_4O_7$) was used; no matrix correction was applied because of the high dilution. All discussion in this paper refers to analyses that have been normalized to 100% on a volatile-free basis with total iron calculated as FeO.

Concentrations of other trace elements, including the rare earth elements (REE), V, Cr, Rb, Sr, Y, Zr, Nb, Cs, Ba, Hf, Ta, Pb, Th, and U were determined by ICP-MS using a Agilent 7900 instrument at the Geological Survey of Japan/AIST. About 100 mg of sample powder was dissolved in a HF-HNO_3 mixture (5:1). After evaporation to dryness, the residues were redissolved with 2% HNO_3 prior to analysis. Reproducibility is better than ±4% [2 standard deviations (SD)] for the REE, Rb and Nb, and better than ±6% (2 SD) for other elements.

For a sample from KS-22-1, trace element concentrations were determined by ICP-MS (iCAP Qc, ThermoFisher Scientific, Bremen, Germany) at the JAMSTEC. Sample preparation followed the procedures of Chang et al. (2003). In brief, an aliquot of 50–100 mg rock powder was digested with a mixture of HF-$HClO_4$, followed by $HClO_4$ and HNO_3. Finally, the residues were dissolved in 2% HNO_3 with trace amount of HF to maintain the stability of elements in solution. ICP-MS analysis signals were normalized using In and Bi as internal standards. Reproducibility of data for JB-2 in this study at JAMSTEC is better than 2% RSD.

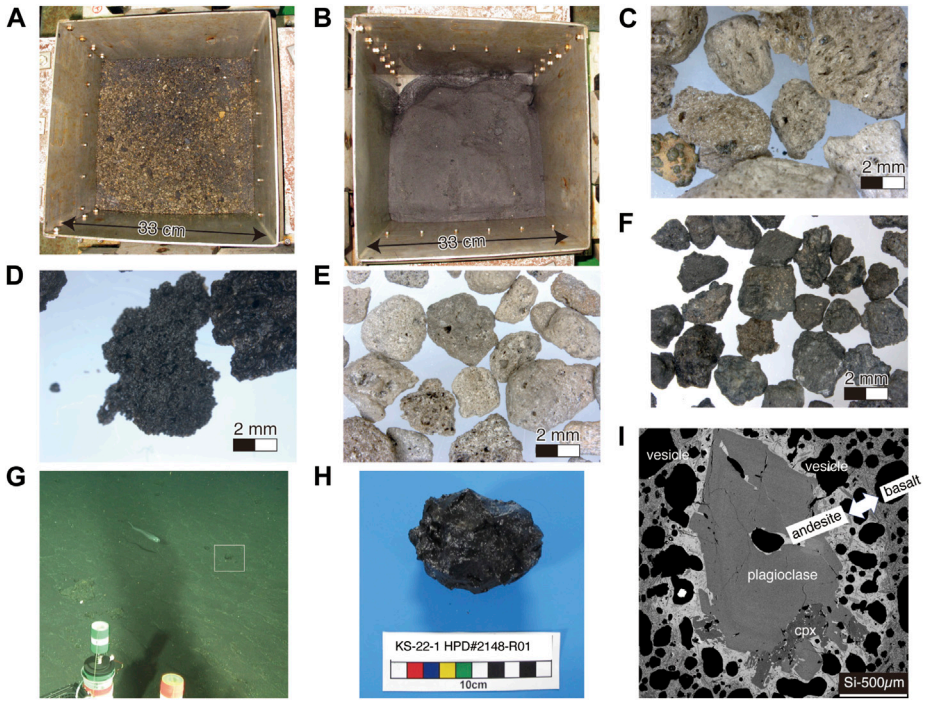

FIGURE 5
(A,B) Seafloor sediments (the latest tephra in December 2020) recovered by the Box Corer whose sites are shown in Figure 3B. The Box Corer covers an area of 0.1 m^2 (33 cm * 33 cm). The seafloor was mostly covered by black tephra (scorias), but some light-colored materials (pumices) were observed along with the scorias. **(A)** BX#01 recovered from 945 m b.s.l. **(B)** BX#02 from 952 m b.s.l. **(C)** Pumices from BX#01. **(D)** Scorias from BX#06 recovered from 1,500 m b.s.l. **(E)** Pumices recovered from a white layer in Figure 4B during HPD#2123. **(F)** Scorias recovered from a black layer just below the white layer in Figure 4B during HPD#2123 at a depth of 2,500 m b.s.l., 15 km in the north of Nishinoshima. **(G)** Seafloor at a depth of 760 m observed during HPD#2148 (Figure 3B) by using ROV Hyper Dolphin in the cruise of KS22-1 cruise in 2022. White rectangle frames recovered sample shown in **(H)**. **(H)** Larger basaltic andesite sample (HPD#2148-R01) collected from the sea floor at the southern slope of Nishinoshima, 3.3 km south of the island. **(I)** Si X-ray map taken from a thin section of sample HPD#2148-R01, which has a whole-rock composition of basaltic andesite. The Si-rich light-colored groundmass is andesitic magma containing Ca-poor plagioclase (An_{44-50}) and clinopyroxene (cpx), which exhibits a mingling texture with the surrounding Si-poor dark-colored groundmass of basaltic magma.

Isotopic compositions of Sr, Nd, and Pb were determined on 200 mg of hand-picked 0.5–1 mm rock chips. The chips were leached in 6 M HCl at 140°C for 1 h prior to dissolution in HF–HNO_3. Sr and Nd isotope ratios were measured on a seven-collector VG Sector 54 mass spectrometer at the Geological Survey of Japan/AIST. Sr was isolated using Sr resin (Eichrom Industries, Illinois). For Nd isotopic analysis, the REE were initially separated by cation exchange before isolating Nd on Ln resin (Eichrom Industries) columns. Sr and Nd isotopic compositions were determined as the average of 150 ratios by measuring ion beam intensities in multidynamic collection mode. Isotope ratios were normalized to $^{86}Sr/^{88}Sr$ = 0.1194 and $^{146}Nd/^{144}Nd$ = 0.7219. Measured values for NBS SRM-987 and JNdi-1 [$^{143}Nd/^{144}Nd$ = 0.512115 (Tanaka et al., 2000)] were $^{87}Sr/^{86}Sr$ = 0.710276 ± 0.000006 (2 SD, n = 4) and $^{143}Nd/^{144}Nd$ = 0.512104 ± 0.000012 (2 SD, n = 4) during the measurement period. Pb was isolated using AG1-X8 200–400 mesh anion exchange resin. Procedural Pb blanks were <30 pg, considered negligible relative to the amount of sample analyzed. Pb isotopic measurements were made in multidynamic collection mode using the double spike technique (Ishizuka et al., 2003; Taylor et al., 2015) (Southampton-Brest-Lead 207–204 spike SBL74) at GSJ/AIST. Natural (unspiked) measurements were made on 60%–70% of collected Pb, giving ^{208}Pb beam intensities of (2.5–3.0) × 10^{-11} A. Fractionation-corrected Pb isotopic compositions and internal errors were obtained by a closed form linear double-spike deconvolution (Johnson and Beard, 1999). The reproducibility of Pb isotopic measurement (external error of 2 SD) by double spike is <200 ppm for all $^{20x}Pb/^{204}Pb$ ratios. Measured values for NBS SRM-981 during the measurement period were $^{206}Pb/^{204}Pb$ = 16.9401 ± 0.0011, $^{207}Pb/^{204}Pb$ = 15.5003 ± 0.0025, and $^{208}Pb/^{204}Pb$ = 36.7236 ± 0.0041.

Electron microprobe analyses were carried out on a JEOL JXA-8500F instrument equipped with five wavelength-dispersive spectrometers (WDS) at JAMSTEC using an accelerating voltage of 15 kV, 10 nA beam current, and 3–5 μm spot diameter. Peak and background counting times were 10 and 5 s, respectively. Calibrations were performed using mineral standards.

Supplementary Table S1 shows major element analyses by XRF, trace element analyses by ICP-MS, and Sr-Nd-Pb isotopic compositions of selected samples.

3 Results

3.1 Major elements

Variation diagrams of wt% SiO_2 vs. major elements and Mg-value of lavas and pyroclastic materials from Nishinoshima and

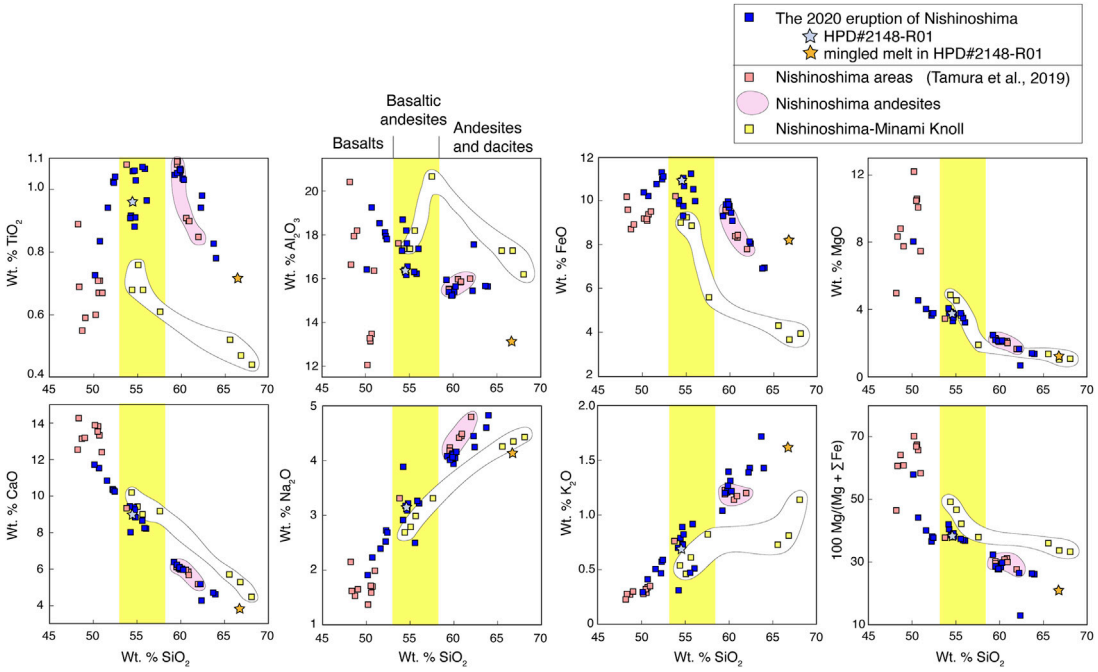

FIGURE 6
Variation diagrams of wt% SiO_2 vs. major elements and Mg-value of lavas and pyroclastic materials from Nishinoshima and surrounding areas. Blue squares indicate new data for submarine deposits of Episode 4 eruptions in 2020 (cruises KR20-E06, KS-21-1, and KS-22-1); stars indicate sample R01 collected during dive HPD#2148. Orange squares indicate samples collected from the Nishinoshima area in 2015 (Tamura et al., 2019), which include older basalts from the NE and SE Knolls; pink shading indicates data range of 1973 eruption products and pre-1973 edifice (Tamura et al., 2019 and references therein). Yellow squares indicate samples collected from Nishinoshima-Minami Knoll in 2015 (Tamura et al., 2019). Compositional boundaries between basalts, basaltic andesites, and andesites and dacites are marked.

surrounding areas (both new and previously published) are shown in Figure 6. Collectively the data range from 48 to 68 wt% SiO_2, 0.7 to 12.2 wt% MgO, and 0.2 to 1.72 wt% K_2O, defining a low-to medium-K suite as defined by Gill (1981). Mg-values range from 13 to 70. The scoria, pumice, and lava fragments from the 2020 eruption (Box Corer and Hyper Dolphin samples) range from 50 to 64 wt% SiO_2, 0.7 to 8 wt% MgO, 0.2 to 1.72 wt% K_2O, and 13 to 58 Mg-values. These values overlap previously reported data for andesite lavas from the Nishinoshima main edifice (59–62 wt% SiO_2) and basalts from the surrounding knolls (48.3–51 wt% SiO_2) (Tamura et al., 2019). Tephras from the 2020 eruption collected on the island were basaltic andesite (54–56 wt% SiO_2; Maeno et al., 2021); thus, basaltic andesites were deemed to be most voluminous and representative of the 2020 eruption (Maeno et al., 2021). However, our submarine samples, which we infer to be from the same 2020 eruption, have a wider compositional variation ranging from basalt (50 wt% SiO_2) to dacite (64 wt% SiO_2). It is possible that a similarly wide range was not recovered from the island itself due to the limited opportunity for sampling.

Lavas from Nishinoshima-Minami Knoll (collected in 2015; Tamura et al., 2019) are distinctly lower in TiO_2 (0.4–0.8 wt%), FeO (3.6–9.2 wt%), Na_2O (2.7–4.4 wt%) and K_2O (0.5–1.1 wt%) and higher in CaO (4–10 wt%) and Mg-values (33–49) than the main Nishinoshima edifice (0.8–1.1 wt% TiO_2, 7–11 wt% FeO, 3–5 wt% Na_2O, 0.6–1.5 wt% K_2O, 4–9 wt% CaO, 30–40 Mg-values) at the same SiO_2 contents in the range of 54–68 wt % SiO_2.

3.2 Trace element ratios

Variation diagrams of wt% SiO_2 vs. selected trace element ratios are shown in Figure 7. These element ratios are used as proxies for mantle and subduction components based on data and interpretations made by Pearce et al. (2005) for the Mariana arc. Accordingly, Ba/Nb is a proxy for total subduction addition, with high Ba/Nb indicating high total subduction addition (since Ba is released over a wide range of subduction temperatures). Similarly, Ba/Th is a proxy for shallow subduction addition (because Ba is mobilized in lower temperature fluids but Th is not), and Th/Nb is a proxy for deep subduction addition (because high temperature melts are required to mobilize Th). Nb/Yb is a proxy for degree of melting in an inverse way, with low Nb/Yb indicating high degrees of melting (because Nb is more incompatible than Yb in the source mantle and incompatible elements are more concentrated in melts resulting from lower degrees of melting) (Pearce et al., 2005). Both La/Sm and Zr/Y could be proxies for partial melt from subducted sediment, with higher La/Sm and Zr/Y indicating higher partial melt content from subducted sediment. Additionally, lower Zr/Y can also indicate higher degrees of mantle melting.

The 2020 basalts have a narrower range of Ba/Nb (100–130) and Ba/Th (330–420) than the previously reported basalts, which range from 40 to 150 and from 150 to 600, respectively. Basalts from the NE Knoll have higher Ba/Nb (~150) and Ba/Th (~600) than those from the SE Knoll (Ba/Nb, 40–57; Ba/Th, 260–350), and the 2020 basalts are plotted intermediate between them.

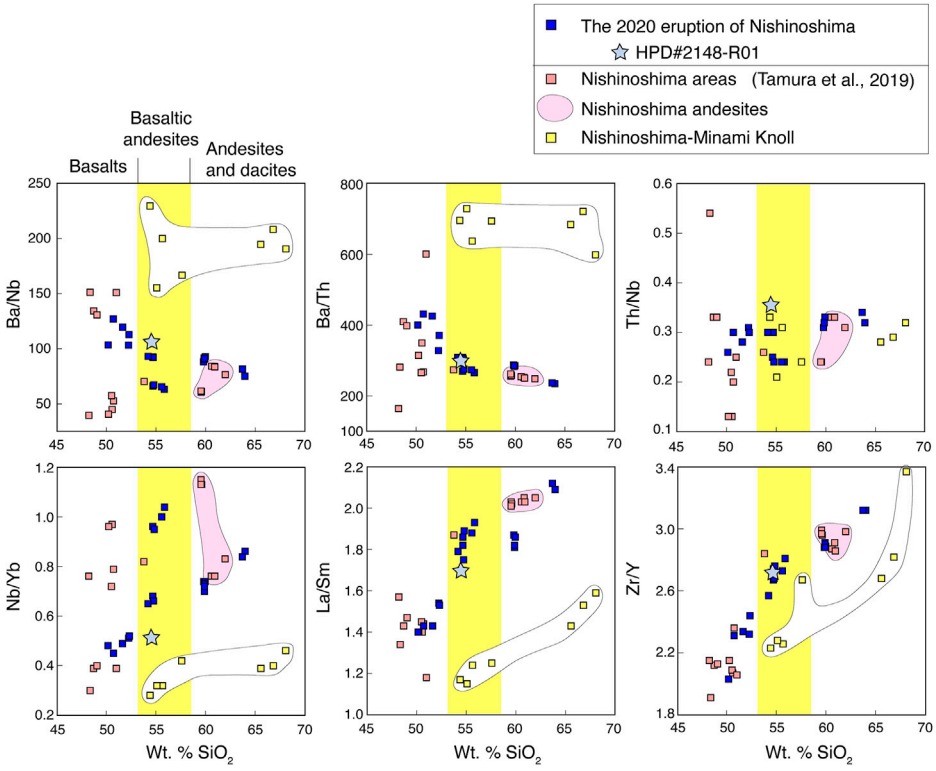

FIGURE 7
Variation diagrams of wt% SiO_2 vs. selected trace element ratios. Blue squares indicate new data for submarine deposits of Episode 4 eruptions in 2020 (cruises KR20-E06, KS-21-1, and KS-22-1); star indicates sample R01 collected during dive HPD#2148. Orange squares indicate samples collected from the Nishinoshima area in 2015 (Tamura et al., 2019), which include older basalts from the NE and SE Knolls; pink shading indicates data range of 1973 eruption products and pre-1973 edifice (Tamura et al., 2019 and references therein). Yellow squares indicate samples collected from Nishinoshima-Minami Knoll in 2015 (Tamura et al., 2019). Compositional boundaries between basalts, basaltic andesites, and andesites and dacites are marked.

Basaltic andesites, andesites, and dacites from the 2020 eruption have Ba/Nb (50–100) and Ba/Th (200–300), which are lower than the 2020 basalts, but similar to Nishinoshima andesites of Tamura et al. (2019). Notably, basaltic andesites and dacites from Nishinoshima-Minami Knoll have higher Ba/Nb (150–230) and Ba/Th (600–730) than those from Nishinoshima and surrounding areas.

The range of Th/Nb (0.24–0.33) of the 2020 eruption is almost similar to the previously reported data around Nishinoshima by Tamura et al. (2019) except for the lowest values of SE Knoll basalts (0.13–0.22) and the highest value (0.54) of the Northern Knoll basalt (DT-1167).

In the 2020 eruption, basaltic andesites have the highest Nb/Yb ranging from 0.51 to 1.04. Andesites and dacites are between 0.70 and 0.86. Basalts range from 0.45 to 0.52. All these values are, however, in the range for the Nishinoshima area reported in Tamura et al. (2019), for which basalt has the lowest value (0.3) and andesite has the highest (1.15). These wide variations in Nb/Yb values make a sharp contrast to Nishinoshima-Minami Knoll, which has generally low Nb/Yb values ranging from 0.28 to 0.46.

In summary, these trace element ratios are similar between the scorias, lava fragments, and pumices from the 2020 eruption and the previously reported andesite lavas from the main Nishinoshima edifice and basalts from the surrounding knolls. However, the lavas from Nishinoshima-Minami Knoll, which is only 8 km south of Nishinoshima island, are distinct from those of the Nishinoshima main body and surrounding knolls.

3.3 Rare earth element (REE) patterns

Figure 8 shows C1 chondrite (McDonough and Sun, 1995)-normalized REE patterns for lavas from the Nishinoshima area. Patterns of basalts from the 2020 eruption (Figure 8A) are similar to patterns of old basalts from the NE Knoll and SE Knoll of Nishinoshima (Figure 3A; Tamura et al., 2019). Basaltic andesites, andesites, and dacites from Nishinoshima (Figure 8B) also exhibit similar patterns between the new samples from the 2020 eruption and the old samples reported in Tamura et al. (2019). Interestingly, a 2015 sample of basaltic andesite from the eastern submarine flank of Nishinoshima (sample KR15-03-R02, Figure 3A), which was reported in Tamura et al. (2019) but not discussed in detail because it was an accidentally sampled rolling stone, has almost the same pattern as the basaltic andesites from the 2020 eruption. Basaltic andesites and dacites from Nishinoshima-Minami Knoll, however, have distinct patterns (Figure 8C). Comparisons between Nishinoshima basalts, Nishinoshima-Minami Knoll, and Nishinoshima andesites and dacites are summarized in Figure 8D.

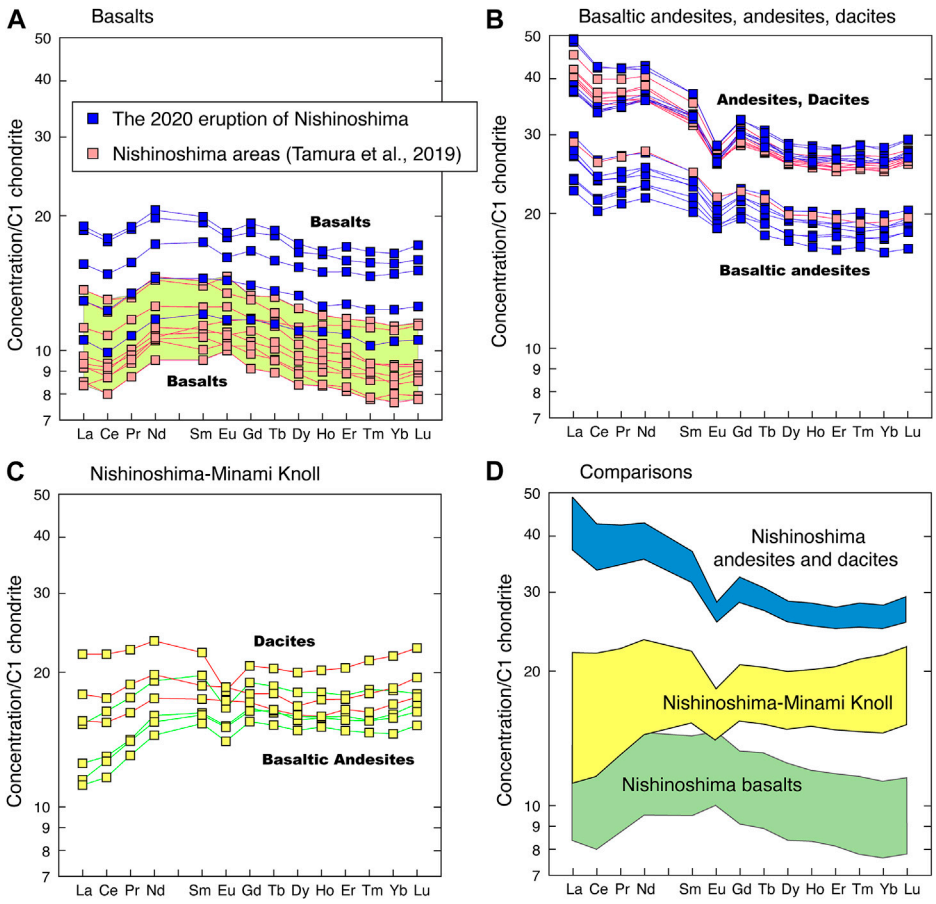

FIGURE 8
C1 chondrite (McDonough and Sun, 1995)-normalized REE patterns for lavas from Nishinoshima area. Blue squares indicate new data for submarine deposits of Episode 4 eruptions in 2020 (cruises KR20-E06, KS-21-1, and KS-22-1). Orange squares indicate samples collected from the Nishinoshima area in 2015 (Tamura et al., 2019), which include older basalts from the NE and SE Knolls. Yellow squares indicate samples collected from Nishinoshima-Minami Knoll in 2015 (Tamura et al., 2019). **(A)** Basalts. **(B)** Basaltic andesites, andesites, and dacites from Nishinoshima. **(C)** Basaltic andesites and dacites from Nishinoshima-Minami Knoll. **(D)** Comparisons between Nishinoshima basalts, Nishinoshima-Minami Knoll, and Nishinoshima andesites and dacites.

3.4 Normal (N)-MORB-normalized trace element patterns

N-MORB (Sun and McDonough, 1989)-normalized trace element patterns of lavas and pyroclastic rocks from the Nishinoshima area are shown in Figure 9. Panels (A), (B), and (C) show basalts, basaltic andesites, and andesites and dacites from the 2020 eruption, respectively, which are compared with the previous data for the Nishinoshima area of Tamura et al. (2019). Panel (D) shows basaltic andesites and dacites from Nishinoshima-Minami Knoll from Tamura et al. (2019).

Basalts of the 2020 eruption (Figure 9A) show the typical signature of subduction zones, being enriched in elements mobile in aqueous fluids and sediment melts (e.g., Rb, Ba, Th, U, K, Pb, and Sr). These basalts are depleted in Nb and Ta, and Zr, Hf, and Ti, which is also typical of subduction zone basalts. These basalts are more differentiated, and thus, the total values are higher, but they are similar and parallel to the previously reported basalts of Tamura et al. (2019).

As suggested by Tamura et al. (2019), the other lava compositions from the Nishinoshima area, including the new 2020 eruption samples, also show the typical signature of subduction zones, enriched in elements mobile in aqueous fluids and sediment melts (e.g., Rb, Ba, Th, U, K, and Pb), but the positive Sr anomalies of the Nishinoshima basalts, basaltic andesites, and Nishinoshima-Minami rocks are absent in the Nishinoshima andesites and dacites.

3.5 SiO_2 vs. La/Sm and Ba/Th vs. La/Sm

$(La/Sm)_N$ is La/Sm normalized to primitive mantle values, which were suggested by Sun and McDonough (1989). $(La/Sm)_N$ can be used as a proxy for partial melt from subducting sediments (Elliott, 2003). Figure 10 shows variation of $(La/Sm)_N$ vs. SiO_2 and Ba/Th for lavas from the Nishinoshima area. Nishinoshima andesites have $(La/Sm)_N$ values ranging from 1.2 to 1.4, which indicate the highest sediment component in this area. Nishinoshima basaltic andesites have values ranging from 1.13 to 1.25, which are plotted between the

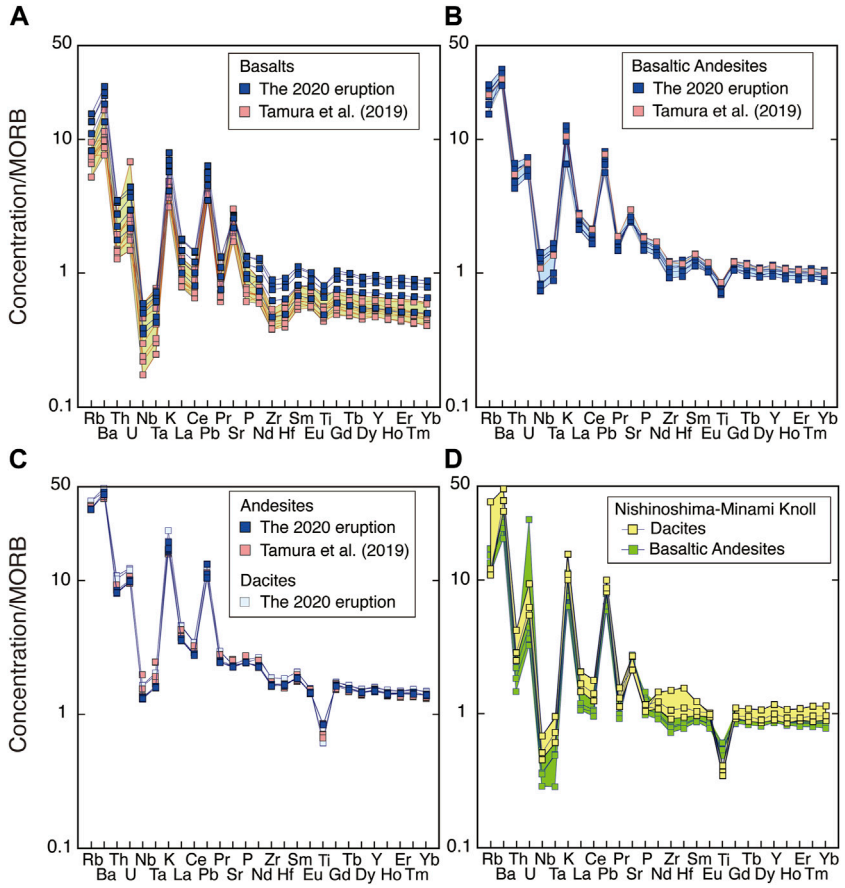

FIGURE 9
Normal (N)-MORB (Sun and McDonough, 1989)-normalized incompatible element patterns of lavas from Nishinoshima area. Blue and white squares indicate new data for submarine deposits of Episode 4 eruptions in 2020 (cruises KR20-E06, KS-21-1, and KS-22-1). Orange squares indicate samples collected from the Nishinoshima area in 2015 (Tamura et al., 2019), which include older basalts from the NE and SE Knolls. Yellow and green squares indicate samples collected from Nishinoshima-Minami Knoll in 2015 (Tamura et al., 2019). **(A)** Basalts. **(B)** Basaltic andesites. **(C)** Andesites and Dacites from Nishinoshima. **(D)** Basaltic andesites and dacites from Nishinoshima-Minami Knoll.

Nishinoshima andesites and basalts (0.76–1.01). Lavas from Nishinoshima-Minami Knoll and Nishinoshima basalts have the lowest $(La/Sm)_N$, ranging from 0.74 to 1.03, and 0.76 to 1.01, respectively, and thus the lowest sediment component in this area.

Ba/Th is used as a proxy for fluid from subducting oceanic crust (Elliott, 2003). Nishinoshima-Minami Knoll lavas have the highest Ba/Th values ranging from 600 to 730, which contrast with Nishinoshima andesites, whose Ba/Th values range from 250 to 280.

3.6 Sr, Nd, and Pb isotope ratios

The new Sr-Nd-Pb isotope ratios of the rocks from the 2020 eruption are plotted along with the data from Tamura et al. (2019) in Figures 11, 12. Basalts from the 2020 eruption have $^{87}Sr/^{86}Sr$ values ranging from 0.70330 to 0.70334, and $^{143}Nd/^{144}Nd$ values ranging from 0.513072 to 0.513087, which are plotted within the Sr-Nd isotopic range (0.70328–0.70360 and 0.513048–0.513131, respectively) of the other basalts reported in the Nishinoshima area (Figure 11). Basalts from the SE knoll (DT-1174) have the highest $^{87}Sr/^{86}Sr$ (0.70360) and the lowest $^{143}Nd/^{144}Nd$ (0.513048) in the Nishinoshima area. $^{87}Sr/^{86}Sr$ and $^{143}Nd/^{144}Nd$ values of Nishinoshima andesites range from 0.70328 to 0.70335 and from 0.51307 to 0.51308, respectively, and those of basaltic andesites are 0.70323–0.70333 and 0.513075–0.513098, respectively. Basaltic andesites have slightly higher $^{143}Nd/^{144}Nd$ than andesites. Nishinoshima-Minami Knoll has $^{87}Sr/^{86}Sr$ and $^{143}Nd/^{144}Nd$ values ranging from 0.70343 to 0.70351 and 0.51311 to 0.513135, respectively, and these are both higher than Nishinoshima andesites and basaltic andesites.

Nishinoshima andesites and basaltic andesites have higher $(La/Sm)_N$ and lower $^{143}Nd/^{144}Nd$ values than Nishinoshima-Minami Knoll (Figure 11), and these values show negative correlations. Basalts have wider $^{143}Nd/^{144}Nd$ values ranging from 0.51305 to 0.51313, but $(La/Sm)_N$ values have a limited range (0.76–1.02).

Figure 12 shows Pb isotope variations. Nishinoshima andesites show a limited range of $^{206}Pb/^{204}Pb$ values, ranging from 18.67 to 18.75, which are positively correlated to $^{87}Sr/^{86}Sr$ from 0.70329 to 0.70335 (Figure 12A), $^{207}Pb/^{204}Pb$ from 15.540 to 15.547 (Figure 12C), and $^{208}Pb/^{204}Pb$ from 38.41 to 38.48 (Figure 12D). Basaltic andesites have slightly wider ranges than andesites in $^{206}Pb/^{204}Pb$, $^{207}Pb/^{204}Pb$, and $^{208}Pb/^{204}Pb$, which are 18.66–18.76,

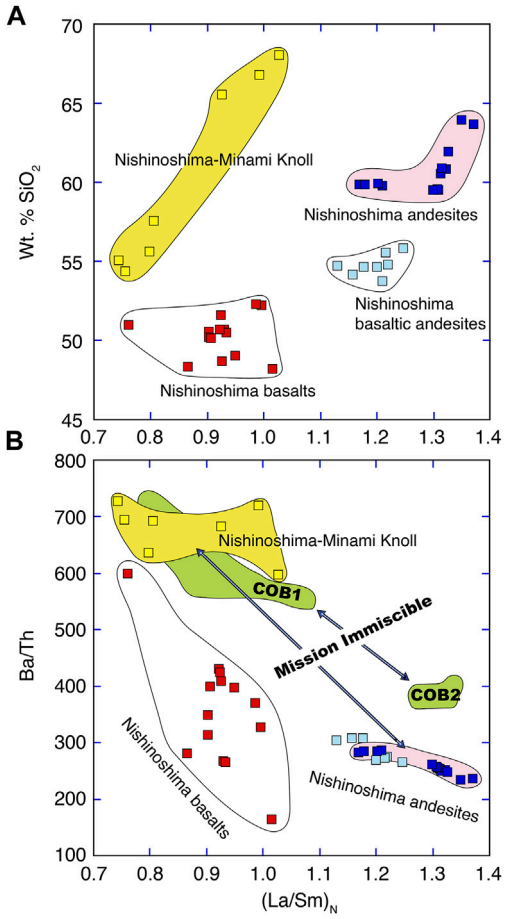

FIGURE 10
Variation of La/Sm normalized to primitive mantle (Sun and McDonough, 1989) vs. SiO_2 **(A)** and Ba/Th **(B)** for lavas from the Nishinoshima area. Samples are grouped by composition and geographical location, regardless of eruption or sampling date. Green COB1 and COB2 fields relate to data from Pagan Volcano in the Mariana arc (Tamura et al., 2014; see main text for details).

15.538–15.548, and 38.394–38.49, respectively. Basalts cover the widest ranges of $^{206}Pb/^{204}Pb$, $^{207}Pb/^{204}Pb$, and $^{208}Pb/^{204}Pb$, ranging from 18.52 to 18.83, from 15.538 to 15.549, and from 38.29 to 38.59, respectively. Nishinoshima-Minami Knoll has the highest $^{206}Pb/^{204}Pb$, $^{143}Nd/^{144}Nd$, and $^{208}Pb/^{204}Pb$ values ranging from 18.80 to 18.86, 0.51311 to 0.513135, 38.48 to 38.56, respectively, which positively correlate each other (Figures 12B, D). Nishinoshima andesites and Nishinoshima-Minami Knoll have similar $^{207}Pb/^{204}Pb$, but Nishinoshima andesites have lower $^{87}Sr/^{86}Sr$, $^{143}Nd/^{144}Nd$, and $^{206}Pb/^{204}Pb$ than those of Nishinoshima-Minami Knoll.

3.7 Petrography of basaltic andesite

HPD#2148-R01 is a key sample of basaltic andesite that was collected from the sea floor at the southern slope of Nishinoshima, 3.3 km south of the island (Figures 3B, 5G), using ROV Hyper Dolphin (HPD#2148) in the cruise of KS-22-1 in 2022. This sample (Figure 5H) represents basaltic andesites erupted in the 2019-2020 eruption, which have similar major element contents (Figure 6) and trace element ratios (Figure 7) to other basaltic andesites from the Nishinoshima area.

This sample is particularly important because it exhibits mingling between basaltic and andesitic magmas (Figure 5I). The major parts of the rock have plagioclase with Ca-rich ($An_{>90}$) cores, clinopyroxene, and olivine phenocrysts with Mg-rich ($Fo_{\sim 83}$) cores within a microlite-rich groundmass. Limited domains have Ca-poor plagioclase (An_{44-50}) accompanying a microlite-poor domain. The volcanic glass in the outer parts in Figure 5I is andesitic and the inner parts are dacitic in composition. These differences in phenocrysts and groundmass compositions suggest the mingling between basaltic and andesitic magmas during the 2020 eruptions.

4 Discussion

4.1 Andesites from Nishinoshima volcano

The andesites that erupted in Episode 4 from 2019 to 2020 overlap with the range of the previous Nishinoshima andesites in terms of major elements (Figure 6), trace element ratios (Figure 7), REE patterns (Figure 8), incompatible trace element patterns (Figure 9), and Sr-Nd-Pb isotopic ratios (Figures 11, 12). Thus, almost the same andesite magmas as historical andesite lavas erupted from Nishinoshima volcano in 2019–2020.

Phenocryst-poor Nishinoshima andesites contain olivine phenocrysts with Fo mol% [100 Mg/(Mg + Fe)] ranging from Fo_{60} to Fo_{86}. Variation in NiO wt% versus Fo mol% for olivine phenocrysts agrees with calculated olivine fractionation trends, which were produced by adding equilibrium olivine compositions into the bulk rock composition iteratively in 1 wt% increments and allowing the bulk rock composition to evolve (Tamura et al., 2019). Additions of 18%–24% equilibrium olivine to Nishinoshima andesites result in primary andesites with ~57 wt% SiO_2 and 9–11 wt% MgO (Tamura et al., 2019). These liquids are in equilibrium with mantle olivines [Fo_{89-91} with 0.4 wt% NiO; see Tamura et al. (2014) for references of mantle olivines]. The estimated primary andesites have higher TiO_2 (0.67–0.75 wt%) and lower CaO (4.2–4.9 wt%) than recently erupted high-Ca boninites from the active Tonga Arc (Cooper et al., 2010), but have an affinity with type-2 low-Ca boninites such as those from the Setouchi area in southwestern Japan (Crawford et al., 1989).

Because of the thin crust (Kodaira et al., 2007), the mantle beneath Nishinoshima could be shallow enough (<1.0 GPa) for plagioclase peridotites to be stable in the mantle source of the Nishinoshima andesites (e.g., Kushiro and Yoder, 1966; Green and Ringwood, 1970; Presnall et al., 2002). Approximately, 10% partial melting of source mantle without Eu anomalies can produce the Eu anomalies of Nishinoshima andesites [$(Eu/Sm)_N < 0.83$ and $(Eu/Gd)_N < 0.92$], when their residues are plagioclase peridotites having 3%–14% plagioclase (Tamura et al., 2019).

4.2 Basalts from Nishinoshima volcano in Episode 4

The activity that started from December 2019 (Episode 4) was intense, with a transition in eruption style from mostly effusive

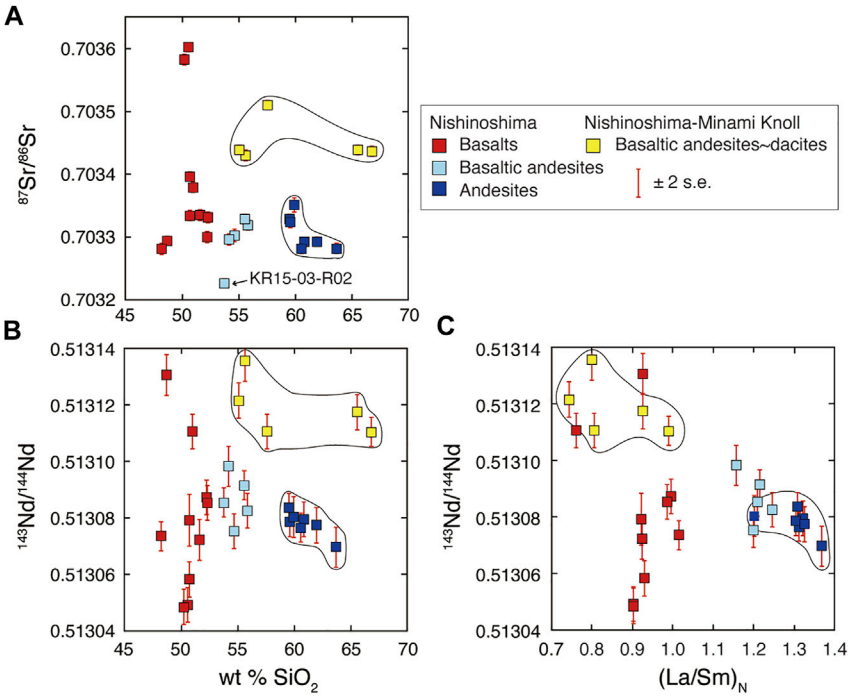

FIGURE 11
(A) $^{87}Sr/^{86}Sr$ vs. SiO_2, **(B)** $^{143}Nd/^{144}Nd$ vs. SiO_2, and **(C)** $^{143}Nd/^{144}Nd$ vs. $(La/Sm)_N$ for lavas from the Nishinoshima area. Samples are grouped by composition and geographical location, regardless of eruption or sampling date.

Strombolian to violent Strombolian in mid-June 2020 that caused a large amount of tephra to fall out over more than several tens of kilometer from the island (Yanagisawa et al., 2020). Although the subaerial samples of this tephra were basaltic andesite in composition (Maeno et al., 2021), our new data for submarine deposits of this tephra (Figures 3B, 4, 5) show that the pyroclastic rocks from Episode 4 range from basalt to dacite (Figures 6, 7). Thus, basalt was a part of the most recently erupted materials. Magma compositions therefore changed from andesite to basaltic andesite and basalt in the middle of June 2020. The small amount of dacite is not discussed in this paper, but could result from partial melting of the existing andesite edifice (Tamura et al., 2009).

Tamura et al. (2019) concluded that small knolls near Nishinoshima including the NE and SE Knolls (Figure 3) consist of old basalts whereas the main body of Nishinoshima consists of new andesites, which were derived from primary basalt and primary andesite magmas from deep and shallow mantle sources, respectively. Old basalt magmas were found spread over a wide Nishinoshima area, but new andesite magmas were concentrated in a smaller area that comprised the main body of Nishinoshima (Tamura et al., 2019). This previous understanding of the sequential and spatially demarcated evolution of Nishinoshima volcano from basalt to andesite magmas has been transformed by the 2020 Episode 4 eruption.

Now, the newest magmas erupted from the Nishinoshima volcanic center are basaltic in composition. Moreover, the new basalt from the eruptive center is distinctly less primitive than the old basalts erupted from the surrounding knolls. Figures 6–9 show major element, trace element ratios, REE patterns, and incompatible element patterns, respectively. Some basalts from the knolls are magnesian, having >10 wt% MgO and higher Mg-numbers than the basalts from the 2020 eruption (Figure 6), but there are no systematic differences in trace element ratios (Figure 7). REE patterns and incompatible trace element patterns also suggest that the 2020 basalts are more differentiated than the old submarine basalts, but their patterns are mostly parallel to the old basalts (Figures 8, 9). Pb-Sr-Nd isotope ratios of the new basalts overlap the old basalts (Figures 11, 12). These lines of evidence suggest that the new and old basalt magmas were derived from either the same, or similar, magma source beneath Nishinoshima. Importantly, however, the basaltic products are heterogeneous in some trace element ratios (i.e., Ba/Nb) and isotopic ratios (i.e., $^{143}Nd/^{144}Nd$) and it is difficult to explain the origin of this heterogeneity.

The basalts have both weakly positive and negative Eu-anomalies, possibly because the source mantle itself can have Eu anomalies. Prinzhofer and Allègre (1985) report systematic negative Eu anomalies in peridotites of the New Caledonia ophiolite (Southwest Pacific). Ulrich et al. (2010) further showed that the ophiolite samples had both negative and positive Eu anomalies ($Eu/Eu^* = 0.33–6.78$).

The key difference between prior eruptions of basalt lavas at Nishinoshima and the 2020 eruption is that the 2020 eruption began as andesite and transitioned to basalt at a vent that normally erupts andesite.

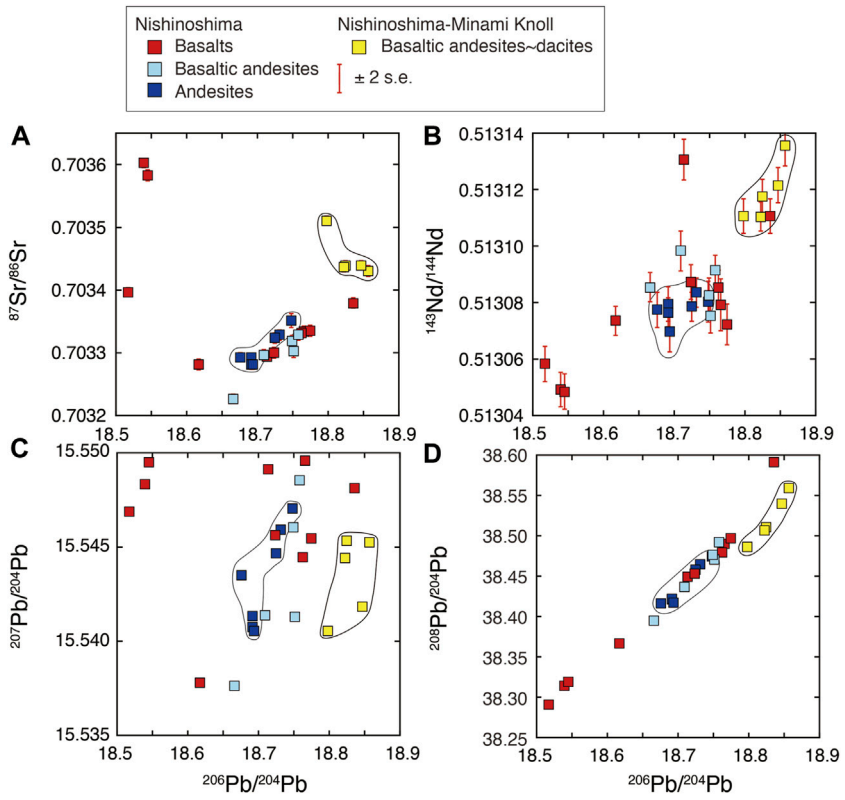

FIGURE 12
(A) $^{87}Sr/^{86}Sr$ vs. $^{206}Pb/^{204}Pb$, **(B)** $^{143}Nd/^{144}Nd$ vs. $^{206}Pb/^{204}Pb$, **(C)** $^{207}Pb/^{204}Pb$ vs. $^{206}Pb/^{204}Pb$, and **(D)** $^{208}Pb/^{204}Pb$ vs. $^{206}Pb/^{204}Pb$ for lavas from the Nishinoshima area. Samples are grouped by composition and geographical location, regardless of eruption or sampling date.

4.3 Basaltic andesites from Nishinoshima volcano in Episode 4

A large amount of the tephra erupted in Episode 4, representing the most voluminous magmas in 2020, were basaltic andesite in composition ranging from 53 to 58 wt% SiO_2 (Maeno et al., 2021). Major element compositions of basaltic andesites from Nishinoshima are intermediate between basalts and andesites (Figure 6). Trace element ratios are similar to those of Nishinoshima andesites (Figure 7).

REE patterns of Nishinoshima basaltic andesites and andesites are mostly parallel, except for negative Eu-anomalies that are strong in andesites but weak in basaltic andesites (Figure 8B). The strong negative Eu-anomalies of the andesites were interpreted to have resulted from their shallow mantle source and plagioclase-bearing residue (plagioclase lherzolite) (Tamura et al., 2019). The basaltic andesites have REE patterns intermediate between basalts and andesites.

Incompatible trace element patterns of Nishinoshima basaltic andesites are also intermediate between basalts and andesites (Figure 9), and positive Sr-anomalies are strong in basalts, weak in basaltic andesites and absent in andesites (Figure 9). However, both basaltic andesites and dacites from Nishinoshima-Minami Knoll have strong positive Sr-anomalies (Figure 9D).

The large amount of basaltic andesite explosively erupted in Episode 4 was the first basaltic andesite that was erupted from the Nishinoshima vent since historical eruptive activity began in 1973. That was unexpected and unusual because Episodes 1, 2, and 3 as well as the previous 1973 episode consisted of andesite eruptions (Maeno et al., 2021). However, this new eruption of basaltic andesite solved a small riddle, which could not be understood in Tamura et al. (2019).

As shown in Figures 6–9, we already reported a basaltic andesite from Nishinoshima in Tamura et al. (2019). This loose boulder stone (KR15-03-R02) was collected at a depth of 2,100 m ESE of Nishinoshima during cruise KR15-03 in 2015 (Figure 3A). This boulder and Episode 4 basaltic andesites are similar in major elements (Figure 6), trace element ratios (Figure 7), REE patterns (Figure 8B), and incompatible trace element patterns (Figure 9B). This boulder, however, has the lowest $^{87}Sr/^{86}Sr$ (0.703227) in the Nishinoshima area (Figure 11A), which is the only difference from the Episode 4 basaltic andesites. Evidently, basaltic andesites of similar composition to those of Episode 4 had previously been erupted from the volcanic center of Nishinoshima during prehistoric (pre-1973) eruptions.

As outlined above, andesites erupted from Nishinoshima are interpreted to have been produced by olivine fractionation of primary andesitic magmas generated at shallow depth whereas older basalts were derived from primary basaltic magmas generated at greater depth (Tamura et al., 2016; Tamura et al., 2019). In this scenario, the chemically intermediate basaltic andesite could be produced by mixing between mantle-derived andesite and

mantle-derived basalt magmas in a magma chamber. It should be noted that the possible end-member basaltic magmas needed to produce the observed basaltic andesite compositions through mixing should have higher Ba/Nb ratios (Figure 7), higher Ba/Th ratios (Figure 10), and higher $^{143}Nd/^{144}Nd$ ratios than some basalt samples presented here, but our data show that geochemically heterogeneous basaltic magmas do exist at Nishinoshima.

Evidence for the proposed mixing between andesite and basalt magmas is seen in sample HPD#2148-R01 (Figure 5I), and a magma mixing scenario is consistent with the eruption sequence of Episode 4 (Maeno et al., 2021). Moreover, the existence of prehistoric basaltic andesite in the main body of Nishinoshima suggests that intrusions of basalt magmas might have happened before and may not be an unusual event for this volcano.

4.4 Nishinoshima-Minami Knoll and "mission immiscible"

Nishinoshima-Minami Knoll is 8 km south of Nishinoshima island and is built on the southern submarine flank of Nishinoshima. Despite this proximity, the lavas from Nishinoshima-Minami Knoll are distinct from those of the Nishinoshima main body and surrounding knolls. Compared with Nishinoshima andesites, Nishinoshima-Minami Knoll is low in TiO_2, FeO, Na_2O, and K_2O, and relatively high in Al_2O_3, CaO, and Mg value (Figure 6). High Ba/Nb and Ba/Th values suggest that the lavas from Nishinoshima-Minami Knoll are enriched in shallow subduction addition (e.g., Elliott, 2003; Pearce et al., 2005), while their low Nb/Yb values suggest a higher degree of mantle melting than Nishinoshima lavas (Figure 7). Moreover, light rare earth element (LREE; La, Ce, Pr, and Nd) concentrations are low in lavas from Nishinoshima-Minami Knoll compared to middle and heavy rare earth elements (MREEs and HREEs), suggesting that subducting sediment does not play an important role in the subduction components of these lavas (Figure 8). Instead, their high $^{87}Sr/^{86}Sr$, $^{143}Nd/^{144}Nd$, $^{206}Pb/^{204}Pb$, and $^{208}Pb/^{204}Pb$ (Figures 11, 12), coupled with high Ba/Th and low La/Sm (Figure 10), indicate sources enriched in hydrous fluids derived from the subducting Pacific Plate (e.g., Elliott, 2003; Pearce et al., 2005).

By contrast, the Nishinoshima andesites have LREE-enriched patterns with negative Eu anomalies that are different from the flat to LREE-depleted patterns of Nishinoshima-Minami Knoll (Figures 8B, C). The MORB-normalized incompatible element patterns (Figure 9) show that the lavas from the Nishinoshima area have the typical signature of subduction zones, enriched in elements mobile in aqueous fluids and sediment melts (e.g., Ba, U, K, and Pb). Interestingly, however, the positive Sr anomalies observed in the Nishinoshima-Minami rocks are absent in the Nishinoshima andesites (Figure 9C). The Nishinoshima andesites have lower $^{87}Sr/^{86}Sr$, $^{143}Nd/^{144}Nd$, $^{206}Pb/^{204}Pb$, and $^{208}Pb/^{204}Pb$ ratios than the Nishinoshima-Minami Knoll lavas (Figures 11, 12), and their combination of low $^{143}Nd/^{144}Nd$ with high La/Sm and low Ba/Th (Figure 10) suggests that their sources are instead enriched in the sediment melt component.

To interpret these differences between the Nishinoshima and Nishinoshima-Minami Knoll lavas, which occur within 8 km of each other, it is useful to make a comparison with a previous study of primitive arc basalt lavas from Pagan Volcano in the Mariana arc (Tamura et al., 2014). At Pagan, two geochemical groups of fresh basalt lavas can be distinguished at similar 10–11 wt% MgO; these erupted recently, at about the same time, and are only 500 m apart. Tamura et al. call these groups COB1 and COB2 (Figure 10B) because the two varieties have similar phenocryst assemblages (clinopyroxene and olivine) but can be distinguished on the basis of their "subduction component"; that is, what has been added from the subducted Pacific plate to their mantle source.

Ba/Nb and Ba/Th variations suggest that COB1 lavas have total and shallow subduction additions (Pearce et al., 2005) that are larger than those for COB2 lavas; meanwhile, Th/Nb and La/Sm indicate that sediment melts are more important for COB2 than for COB1. The negative correlation between Ba/Nb and Nb/Yb suggests that both total subduction addition and degree of melting of the COB1 source are higher than for the COB2 source. The higher total subduction addition might itself have resulted in a higher degree of melting of the COB1 mantle source; importantly, the subduction addition that caused higher degrees of melting of the COB1 source was mostly hydrous fluid, not sediment melt.

The alternative explanation—that COB1 and COB2 compositions reflect mixing between two endmembers, of a single subduction component and a single mantle component—is shown to be unlikely on the basis of their Pb isotope ratios, which do not define a linear trend in Pb isotope space. Instead, Tamura et al. (2014) suggest that Pb from subducted sediment is important for COB2 lavas, but Pb in aqueous fluid is more important for COB1 lavas. Together these lines of evidence suggest that aqueous fluid and sediment melt coexist when they are released from the subducting slab (Mibe et al., 2011; Kawamoto et al., 2012). These slab components can then be added separately to the source mantle, independently generating COB1 and COB2 magmas. The "mission" of a subducted slab is to add subduction components to the overlying mantle wedge to produce arc magmas. Thus, this coexistence of fluid and melt was referred to as "Mission Immiscible" (Tamura et al., 2014).

This model of separate addition of immiscible fluid and sediment melt components to the source mantle, resulting in independent generation of magmas with different compositions, can be applied to the case of Nishinoshima. Accordingly, lavas from Nishinoshima-Minami Knoll (with higher Ba/Th) derive from source mantle enriched in fluid from altered oceanic crust, whereas Nishinoshima andesites (with higher La/Sm) derive from source mantle enriched in partial melt from subducted sediment (Figure 10B).

Green et al. (2004) suggest that depleted mantle sources may be fertilized by slab-derived carbonatite fluid, which enriches CaO relative to Al_2O_3 in the primary magma derived from the mantle source. Evidence for carbonatite metasomatism in spinel peridotite xenoliths is reported from western Victoria, Australia (Yaxley et al., 1998). The model of Green et al. (2004) could explain the enigmatic enrichment of CaO in COB1 and Nishinoshima-Minami Knoll lavas compared to COB2 and Nishinoshima lavas (Figure 6), respectively, and thus the mantle source of COB1 and Nishinoshima-Minami Knoll might have been fertilized by slab-derived hydrous carbonatite fluid.

Moreover, carbonatite fluid and silicate melt are immiscible, and the miscibility gap expands with increasing pressure and decreasing temperature (e.g., Mattey et al., 1990; Brooker and Kjarsgaard,

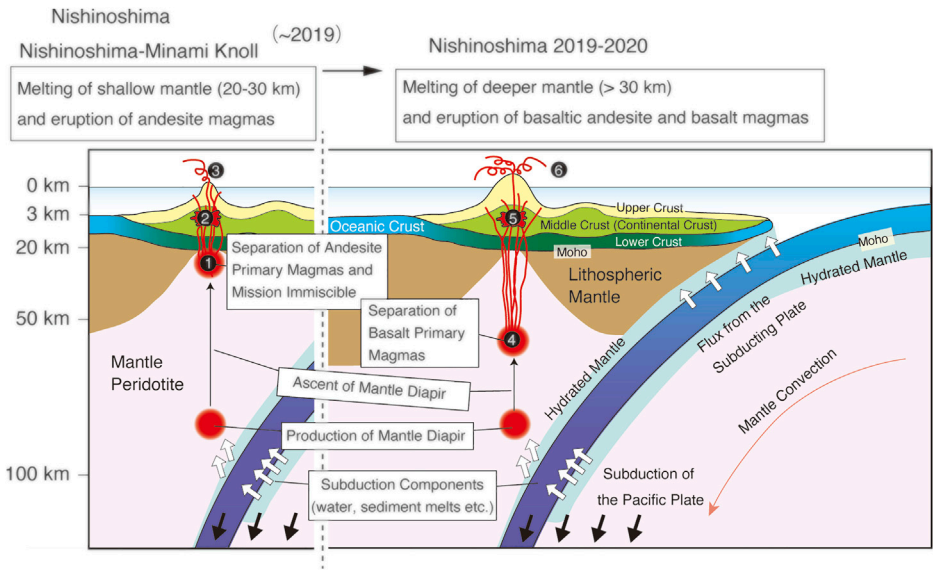

FIGURE 13
Schematic diagram showing the genesis of andesite magmas before 2019 and the genesis of basalt magmas and subsequent mixing with andesite magmas between 2019 and 2020. 1, mantle melting beneath thin crust (low pressure) and production of primary andesite. The "Mission Immiscible" process (Tamura et al., 2014) produced two different primary andesites in the Nishinoshima area (Nishinoshima main body and Nishinoshima-Minami Knoll); 2, efficient olivine fractionation from primary andesite magma in the crust (Tamura et al., 2019); 3, eruption of Nishinoshima andesites; 4, mantle melting at higher pressure and production of primary basalt, which is followed by assimilation of pyroxenes and fractional crystallization of olivines during ascent to the crust (AFC in the mantle, Tamura et al., 2019); 5, ascending basalt magma pushes the existing andesite magma out of the reservoir and then mixes with the andesite magma; 6, extrusion of andesite lava flows in 2019, followed by explosive eruptions of basalt and basaltic andesite in 2020.

2011). The hydrous fluid and sediment melt components are suggested to be immiscible, thus the former could be hydrous carbonatite fluid (Tamura et al., 2014). This immiscibility can make it possible for magmas derived from partial melting of source mantle affected by each component to coexist in the same volcano. Thus, magmas enriched in a sediment component (COB2/Nishinoshima andesites, with high La/Sm and low Ba/Th; Figure 10) and magmas enriched in a hydrous fluid (carbonatite) component (COB1/Nishinoshima-Minami Knoll, with low La/Sm and high Ba/Th), can be erupted within close proximity to each other—within 500 m at Pagan Volcano and at a distance of 8 km in the case of Nishinoshima and Nishinoshima-Minami Knoll.

In summary, primary magmas of Nishinoshima andesites and Nishinoshima-Minami Knoll lavas are derived from the partial melting of plagioclase peridotites at relatively low pressures under the thin crust (Tamura et al., 2019), to which the process of "Mission Immiscible" adds a subduction component of either sediment melt (yielding Nishinoshima andesites) or hydrous carbonatite fluid (yielding Nishinoshima-Minami Knoll basaltic andesites and dacites).

4.5 Evolution of magmas in Nishinoshima

Prior to the construction of Nishinoshima submarine volcano (~1 Ma), basalts erupted from the knolls that surround Nishinoshima (Tamura et al., 2019). Here we present a schematic diagram (Figure 13) to summarize the genesis of andesite magmas before 2019 and the genesis of basalt magmas and subsequent mixing with andesite magmas between 2019 and 2020.

The thin crust underlying Nishinoshima volcano is only 21 km thick (Kodaira et al., 2007). Andesite magmas with Eu anomalies (Figure 8B) can be produced by ~10% partial melting of source mantle without Eu anomalies when their residues are plagioclase peridotites having 3%–14% plagioclase (Tamura et al., 2019) (Figure 13, no. 1).

The "Mission Immiscible" process (Tamura et al., 2014) produced two different primary andesites in the Nishinoshima area (Nishinoshima main body and Nishinoshima-Minami Knoll), through enrichment in immiscible subduction components consisting of silicate melt (sediment melt) and hydrous carbonate fluid (carbonatite), respectively (Figure 13, no. 1). Immiscible subduction components result in mantle melting separately: Nishinoshima summit and Nishinoshima-Minami Knoll are only 8 km apart.

Efficient olivine fractionation from primary andesite magma in the crust produced Nishinoshima andesites (Tamura et al., 2019) (Figure 13, no. 2), which erupt from the summit of the volcano (Nishinoshima island) (Figure 13, no. 3).

Mantle melting at higher pressure produces primary basalt magmas, which is followed by assimilation of pyroxenes and fractional crystallization of olivines during ascent to the crust (AFC in the mantle, Tamura et al., 2019) (Figure 13, no. 4). Because old and new basalts are chemically similar, and because basaltic andesite, which is deemed to have resulted from mixing of basalt and andesite magmas, erupted prehistorically, it is possible that basalt magmas have been generated throughout the entire history of Nishinoshima, but their eruption center moved to Nishinoshima island in 2020.

Ascending basalt magma pushed the existing andesite magma out of the reservoir, resulting in continuous extrusion of andesite lava flows in 2019. As the ascending basalt magma interacted with the andesite magma some basaltic andesite was produced by magma mixing within the reservoir and/or conduit (Figure 13, no. 5). Explosive eruptions of basaltic andesite and basalt subsequently occurred in 2020 (Figure 13, no. 6). The explosivity is possibly related to the hydrous fluid and/or melt components from the subduction zone.

5 Conclusion

Analysis of submarine deposits has revealed that the 2020 eruption of Nishinoshima consisted of basalt, basaltic andesite, andesite, and dacite magmas. The andesites are similar to those which have erupted from the island since 1973. Nishinoshima andesite primary magmas originate directly from the mantle as a result of shallow and hydrous melting of plagioclase peridotite (Tamura et al., 2019).

The 2020 basalts are comparable to the older previously erupted basalts in the surrounding knolls reported in Tamura et al. (2019). Thus, basalt magmas could have been generated throughout the entire history of Nishinoshima, but their eruption center moved to the island summit in 2020.

In Episode 4, continuous extrusion of andesite lava flows in 2019 was followed by explosive eruptions of basalt and basaltic andesite in 2020. Apparently, ascending basalt magma pushed the existing andesite magma out of the reservoir in Episode 4 and then mixed with the andesite magma to produce basaltic andesite.

Basaltic andesites, which are similar to those of Episode 4, had previously been erupted from the volcanic center of Nishinoshima during prehistoric (pre-1973) eruptions.

Nishinoshima and Nishinoshima-Minami Knoll have distinct subduction components: the former is sediment melt and the latter is hydrous carbonatite fluid. The "Mission Immiscible" process of Tamura et al. (2014) could explain the production of different primary andesite magmas in the shallow mantle beneath Nishinoshima at a lateral distance of only ~8 km.

Generally, silicic volcanism tends to be more explosive than mafic (basaltic) eruptions. However, in oceanic arcs, basaltic volcanism can be more explosive than andesite volcanism.

Data availability statement

The original contributions presented in the study are included in the article/Supplementary Material, further inquiries can be directed to the corresponding author.

Author contributions

YT prepared the manuscript with feedback and contribution from all the coauthors. OI and QC, TS, and KY performed ICP-MS and isotopes, XRF, and EPMA analyses, respectively. All authors listed have made a substantial, direct, and intellectual contribution to the work and approved it for publication.

Funding

This work was supported by JSPS KAKENHI Grant Numbers JP17H02987 and JP21H01195.

Acknowledgments

Sampling of volcanic products from Nishinoshima were carried out in cooperation with shipboard scientists and technical personnel on multiple research vessels (Kairei, Natsushima, and Shinseimaru). Calvin Miller, Sean O'Donnell, and Takeshi Kuritani are thanked for their helpful comments, which improved the paper very much. Kristen Fauria and Valerio Acocella are thanked for the editorial handling.

Conflict of interest

The authors declare that the research was conducted in the absence of any commercial or financial relationships that could be construed as a potential conflict of interest.

Publisher's note

Supplementary material

The Supplementary Material for this article can be found online at: https://www.frontiersin.org/articles/10.3389/feart.2023.1137416/full#supplementary-material

References

Aoki, H., and Ossaka, J. (1974). *A mystery of submarine volcanoes – the exploration records of Nishinoshima (kaiteikazan No nazo)*. Tokyo: Tokai Univ. Press, 250.

Aoki, H., Utsunomiya, Y., Okitsu, H., Kawakami, M., Nakajima, I., and Ichikawa, M. (1983). Petrochemistry of the Nishinoshima islands. *La Mer*. 22, 248–256.

Brooker, R. A., and Kjarsgaard, B. A. (2011). Silicate-carbonate liquid immiscibility and phase relations in the system SiO_2-Na_2O-Al_2O_3-CaO-CO_2 at 0.1-2.5 GPa with applications to carbonatite Genesis. *J. Petrology* 52, 1281–1305. doi:10.1093/petrology/egq081

Chang, Q., Shibata, T., Shinotsuka, K., Yoshikawa, M., and Tatsumi, Y. (2003). Precise determination of trace elements in geological standard rocks using inductively coupled plasma mass spectrometry (ICP-MS). *Front. Res. Earth Evol.* 1, 357–362.

Cooper, L. B., Plank, T., Arculus, R. J., Hauri, E. H., Hall, P. S., and Parman, S. W. (2010). High-Ca boninites from the active Tonga Arc. *J. Geophys. Res.* 115, B10206. doi:10.1029/2009JB006367

Crawford, A. J., Falloon, T. J., and Green, D. H. (1989). "Classification, petrogenesis and tectonic setting of boninites," in *Boninites and related rocks*. Editor A. J. Crawford (London: Unwin Hyman), 1–49.

Elliott, T. (2003). "Tracers of the slab," in *Inside the subduction factory*. Editor J. Eiler (Geophysical Monograph, American Geophysical Union), 138, 23–45.

Gill, J. B. (1981). *Orogenic andesites and plate tectonics*. Berline: Springer, 390.

Green, D. H., and Ringwood, A. E. (1970). Mineralogy of peridotitic compositions under upper mantle conditions. *Phys. Earth Planet. Interiors* 3, 359–371. doi:10.1016/0031-9201(70)90076-2

Green, D. H., Schmidt, M. W., and Hibberson, W. O. (2004). Island-arc ankaramites: Primitive melts from fluxed refractory lherzolitic mantle. *J. Petrology* 45, 391–403. doi:10.1093/petrology/egg101

Ishizuka, O., Taylor, R. N., Milton, J. A., and Nesbitt, R. W. (2003). Fluid–mantle interaction in an intra-oceanic arc: Constraints from high-precision Pb isotopes. *Earth Planet. Sci. Lett.* 211, 221–236. doi:10.1016/S0012-821X(03)00201-2

Ishizuka, O., Taylor, R. N., Yuasa, M., Milton, J. A., Nesbitt, R. W., Uto, K., et al. (2007). Processes controlling along-arc isotopic variation of the southern Izu-Bonin arc. *Geochem. Geophys. Geosystems* 8, Q06008. doi:10.1029/2006GC001475

Johnson, C. M., and Beard, B. L. (1999). Correction of instrumentally produced mass fractionation during isotopic analysis of Fe by thermal ionization mass spectrometry. *Int. J. Mass Spectrom.* 193, 87–99. doi:10.1016/s1387-3806(99)00158-x

Kaneko, T., Maeno, F., Ishihara, M., Yasuda, A., Ohminato, T., Nogami, K., et al. (2022). Episode 4 (2019-2020) Nishinoshima activity: Abrupt transitions in the eruptive style observed by image datasets from multiple satellites. *Earth Planet Space* 74, 34. doi:10.1186/s40623-022-01578-6

Kaneko, T., Maeno, F., Yasuda, A., Takeo, M., and Takasaki, K. (2019). The 2017 Nishinoshima eruption: Combined analysis using himawari-8 and multiple high-resolution satellite images. *Earth Planet Space* 71, 140. doi:10.1186/s40623-019-1121-8

Kawamoto, T., Kanzaki, M., Mibe, K., Matsukage, K. N., and Ono, S. (2012). Separation of supercritical slab-fluids to form aqueous fluid and melt components in subduction zone magmatism. *PNAS* 109, 18695–18700. doi:10.1073/pnas.1207687109

Kodaira, S., Sato, T., Takahashi, N., Miura, S., Tamura, Y., Tatsumi, Y., et al. (2007). New seismological constraints on growth of continental crust in the Izu-Bonin intra-oceanic arc. *Geology* 35, 1031–1034. doi:10.1130/g23901a.1

Kushiro, I., and Yoder, H. S., Jr. (1966). Anorthite-forsterite and anorthite-enstatite reactions and their bearing on the basalt-eclogite transformation. *J. Petrology* 7, 337–362. doi:10.1093/petrology/7.3.337

Maeno, F., Nakada, S., and Kaneko, T. (2016). Morphological evolution of a new volcanic islet sustained by compound lava flows. *Geology* 44 (4), 259–262. doi:10.1130/G37461.1

Maeno, F., Yasuda, A., Hokanishi, N., Kaneko, T., Tamura, Y., Yoshimoto, M., et al. (2021). Intermittent growth of a newly-born volcanic island and its feeding system revealed by geological and geochemical monitoring 2013–2020, Nishinoshima, Ogasawara, Japan. *Front. Earth Sci.* 9, 773819. doi:10.3389/feart.2021.773819

Mattey, D. P., Taylor, W. R., Green, D. H., and Pillinger, C. T. (1990). Carbon isotopic fractionation between CO_2 vapour, silicate and carbonate melts: An experimental study to 30 kbar. *Contributions Mineralogy Petrology* 104, 492–505. doi:10.1007/bf01575626

McDonough, W. F., and Sun, S.-S. (1995). The composition of the Earth. *Chem. Geol.* 120, 223–253. doi:10.1016/0009-2541(94)00140-4

Mibe, K., Kawamoto, T., Matsukage, K. N., Fei, Y., and Ono, S. (2011). Slab melting versus slab dehydration in subduction-zone magmatism. *PNAS* 108, 8177–8182. doi:10.1073/pnas.1010968108

Osaka, J. (1973). On the submarine eruption of Nishinoshima. *Bull. Volcanol. Soc. Jpn.* 18, 97–98.

Osaka, J. (1974). On the activity and development of Nishinoshima volcano, bonin islands. *J. Geogr. (Chigaku Zasshi)* 83, 61–69.

Osaka, J., Ohira, Y., and Minato, I. (1974). On the submarine eruption of Nishinoshima (3). *Bull. Volcanol. Soc. Jpn.* 19, 37–38.

Osaka, J. (1975). On the activity and observation of volcano Nishinoshima (2). *Chishitsu News* 246, 1–9.

Pearce, J. A., Stern, R. J., Bloomer, S. H., and Fryer, P. (2005). Geochemical mapping of the Mariana arc-basin system: Implications for the nature and distribution of subduction components. *Geochem. Geophys. Geosystems* 6. doi:10.1029/2004GC000895

Presnall, D. C., Gudfinnsson, G. H., and Walter, M. J. (2002). Generation of mid-ocean ridge basalts at pressures from 1 to 7 GPa. *Geochimica Cosmochimica Acta* 66, 2073–2090. doi:10.1016/s0016-7037(02)00890-6

Prinzhofer, A., and Allègre, C. J. (1985). Residual peridotites and the mechanisms of partial melting. *Earth Planet. Sci. Lett.* 74, 251–265. doi:10.1016/0012-821x(85)90025-1

Sun, S.-S., and McDonough, W. F. (1989). Chemical and isotopic systematics of oceanic basalts: Implications for mantle composition and processes. *Geol. Soc. Lond. Spec. Publ.* 42, 313–345. doi:10.1144/gsl.sp.1989.042.01.19

Tamura, Y., Gill, J. B., Tollstrup, D., Kawabata, H., Shukuno, H., Chang, Q., et al. (2009). Silicic magmas in the Izu-Bonin oceanic arc and implications for crustal evolution. *J. Petrology* 50, 685–723. doi:10.1093/petrology/egp017

Tamura, Y., Ishizuka, O., Sato, T., and Nichols, A. R. L. (2019). Nishinoshima volcano in the Ogasawara arc: New continent from the ocean? *Isl. Arc* 28, e12285. doi:10.1111/iar.12285

Tamura, Y., Ishizuka, O., Stern, R. J., Nichols, A. R. L., Kawabata, H., Hirahara, Y., et al. (2014). Mission immiscible: Distinct subduction components generate two primary magmas at Pagan Volcano, Mariana arc. *J. Petrology* 55, 63–101. doi:10.1093/petrology/egt061

Tamura, Y., Sato, T., Fujiwara, T., Kodaira, S., and Nichols, A. (2016). Advent of continents: A new hypothesis. *Sci. Rep.* 6, 33517. doi:10.1038/srep33517

Tanaka, T., Togashi, S., Kamioka, H., Amakawa, H., Kagami, H., Hamamoto, T., et al. (2000). JNdi-1: A neodymium isotopic reference in consistency with LaJolla neodymium. *Chem. Geol.* 168, 279–281. doi:10.1016/S0009-2541(00)00198-4

Tani, K., Kawabata, H., Chang, Q., Sato, K., and Tatsumi, Y. (2005). Quantitative analyses of silicate rock major and trace elements by X-ray fluorescence spectrometer: Evaluation of analytical precision and sample preparation. *Front. Res. Earth Evol.* 2, 1–8.

Taylor, R. N., Ishizuka, O., Michalik, A., Milton, J. A., and Croudace, I. W. (2015). Evaluat-ing the precision of Pb isotope measurement by mass spectrometry. *J. Anal. At. Spectrom.* 30, 198–213. doi:10.1039/c4ja00279b

Turner, S., Bourdon, B., and Gill, J. (2003). "Insights into magma Genesis at convergent margins from U-series isotopes," in *Uranium-series geochemistry*. Editors B. Bourdon, G. M. Henderson, C. C. Lundstrom, and S. P. Turner (Mineralogical Society of America and Geochemical Society, Reviews in Mineralogy and Geochemistry), 52, 255–315.

Ulrich, M., Picard, C., Guillot, S., Chauvel, C., Cluzel, D., and Meffre, S. (2010). Multiple melting stages and refertilization as indicators for ridge to subduction formation: The New Caledonia ophiolite. *Lithos* 115, 223–236. doi:10.1016/j.lithos.2009.12.011

Umino, S., and Nakano, S. (2007). *Geology of the Chichijima retto district, quadrangle series, 1:50,000*. Tsukuba: Geological Survey of Japan, AIST.

Yanagisawa, H., Iino, H., Ando, S., Takagi, A., and Oikawa, T. (2020). Violent strombolian eruption from June to August 2020 of Nishinoshima island, Ogasawara islands, Japan. *Bull. Vol. Soc. Jpn.* 65, 119–124.

Yaxley, G. M., Green, D. H., and Kamenetsky, V. (1998). Carbonatite metasomatism in the southeastern Australian Lithosphere. *J. Petrology* 39, 1917–1930. doi:10.1093/petroj/39.11-12.1917

Yoshida, K., Tamura, Y., Sato, T., Hanyu, T., Usui, Y., Chang, Q., et al. (2022). Variety of the drift pumice clasts from the 2021 Fukutoku-Oka-no-Ba eruption, Japan. *Isl. Arc* 31, e12441. doi:10.1111/iar.12441